

High-pressure Raman spectroscopic studies of FeS₂ pyrite

A. K. KLEPPE¹ AND A. P. JEPHCOAT^{1,2}

¹ Department of Earth Sciences University of Oxford, Parks Road, Oxford OX1 3PR, UK

² Diamond Light Source, Rutherford Appleton Laboratory, Chilton, Didcot, Oxfordshire OX11 0QX, UK

ABSTRACT

We report micro-Raman spectroscopic studies of FeS₂ pyrite in the diamond-anvil cell under hydrostatic and non-hydrostatic conditions to 55 GPa at room temperature. Four out of five Raman-active modes are resolved with helium as a pressure-transmitting medium to highest pressures. The fifth mode, T_g(2) [377 cm⁻¹], is weak and unresolved lying ~2 cm⁻¹ from the intense A_g mode [379 cm⁻¹] at 1 bar. We observe an increase in the separation of the E_g [344 cm⁻¹] and T_g(1) [350 cm⁻¹] modes under compression. All observed frequencies increase continuously with increasing pressure showing no evidence for a structural phase transition in accord with both X-ray diffraction and shock-wave studies. The A_g and T_g(1) modes gain significantly in intensity relative to the E_g mode with increasing pressure probably resulting from Raman resonance effects. The T_g(3) mode [430 cm⁻¹] broadens unusually compared to the other pyrite modes with pressure. The Raman data are consistent with a contraction of the S–S and Fe–S bonds under pressure. The main effect of non-hydrostatic conditions on the Raman modes is a strong pressure-induced broadening; the pressure-dependence of the frequencies and relative intensities are not affected within the error of the measurements.

KEYWORDS: FeS₂, pyrite, Raman spectroscopy, high pressure, diamond-anvil cell.

Introduction

THE transition metal dichalcogenide FeS₂, pyrite, is the most abundant of the sulphide minerals and common in a variety of geological environments. Strong geophysical interest in its physical and chemical properties under high pressures and high temperatures has arisen in the context of the Fe–S system's possible role in core formation, evolution and composition. It motivated studies of the equation of state (EOS) of pyrite, its structural stability, elasticity and shear strength (e.g. Merkel *et al.*, 2002; Ahrens and Jeanloz, 1987; Jephcoat, 1985). Pyrite appears structurally stable to the highest pressures and temperatures: static compression experiments to 50 GPa and shock compression data to 320 GPa yielded no evidence for a structural phase transition in this mineral. Ahrens and Jeanloz (1987) suggested that the

stability of FeS₂ pyrite might be due to the low-spin 3d-orbital configuration of Fe²⁺. Diamond-anvil cell studies have shown that the EOS of pyrite depends strongly on the degree of non-hydrostatic stress in the sample (Merkel *et al.*, 2002; Jephcoat, 1985). This study of pyrite is also motivated by interest in its electronic properties and the archetypal nature of dichalcogenides. FeS₂ pyrite is a semiconductor with an indirect band gap between occupied and unoccupied states of ~0.9 eV (e.g. Ferrer *et al.*, 1990). Its electronic properties are strongly influenced by a complex interplay of largely covalent S–S bonds and mainly ionic Fe–S bonds (Cervantes *et al.*, 2002). The possible use of pyrite as a solar cell and solid-state battery material has stimulated numerous theoretical and experimental studies of its electronic properties, in particular of its band gap (Cervantes *et al.*, 2002; Opahle *et al.*, 1999; Eyert *et al.*, 1998). In the most recent study, Cervantes *et al.* (2002) demonstrated with optical absorption spectroscopy that the indirect energy gap of pyrite decreases at a rate of $1.13(9) \times 10^{-2}$ eV/GPa with increasing pressure remaining

* E-mail: annettek@earth.ox.ac.uk

DOI: 10.1180/0026461046830196

indirect to at least 28 GPa. Linear extrapolation of the decrease of the band gap to pressures above 28 GPa yielded a band gap closure and hence metallization pressure of 80(8) GPa.

The structure of FeS₂ pyrite is cubic, space group Pa $\bar{3}$ with four formula units per unit cell (e.g. Stevens *et al.*, 1980). The Fe atoms occupy the sites of a face-centered cubic sublattice and the S atoms are arranged in dumb-bell pairs along $\langle 111 \rangle$ directions located at the mid-points of the cube's edges and body centre. Each Fe atom is coordinated by six nearest-neighbour S atoms in a distorted octahedron and each S atom is bonded to three Fe and one other sulphur atom forming a distorted tetrahedron. The FeS₆ octahedra are linked by corner sharing. The pyrite structure is fully characterized by the lattice constant $a = 5.4160(2)$ Å and the Wyckoff parameter $x = 0.385$ Å. The number and symmetries of the Raman and infrared-active modes of pyrite have been predicted using group theoretical methods (Lutz and Willich, 1974). The irreducible representation of the vibrations of FeS₂ pyrite is $\Gamma = A_g + E_g + 3T_g + 2A_u + 2E_u + 6T_u$. The gerade vibrations ($A_g + E_g + 3T_g$) are all active in the first-order Raman spectrum; the ungerade modes $5T_u$ are infrared active whereas the ($2A_u + 2E_u$) modes and the rigid lattice translations (T_u) are optically inactive. The Raman active modes comprise one totally symmetric mode (A_g), one doubly degenerate mode (E_g), and three triply degenerate modes (T_g). The A_g and $T_g(2)$ mode correspond to in-phase and out-of-phase stretching vibrations of the S₂ dumb-bells, respectively (Fig. 1). In the E_g librational mode the S atoms are displaced perpendicular to the S–S bond axis. $T_g(2)$ and $T_g(3)$ correspond to various librational and stretching motions or their combinations (Sourisseau *et al.*, 1991). The Raman-active modes involve only movements of the S atoms, and therefore the phonon frequencies give information on the forces determining the stretching and librational motions of the S₂ units.

Ambient Raman and IR spectra of FeS₂ pyrite have been published (e.g. Mernagh and Trudu, 1993; Anastassakis and Perry, 1976; Ushioda, 1972). The early Raman studies on FeS₂ had low resolution and Anastassakis and Perry (1976), in addition, reported sample temperatures above 300 K due to absorption of the incident laser beam. This led to uncertainties in both the number and the position of the FeS₂ modes. In most studies only three modes were observed (Mernagh and Trudu, 1993; Anastassakis and Perry, 1976;

Ushioda, 1972). Vogt *et al.* (1983) were the first to report a complete, ambient Raman spectrum of FeS₂ from polarized Raman measurements with four different scattering configurations. Light-scattering studies of opaque minerals at high-pressures are rare. Takahashi *et al.* (1985) reported a positive pressure dependence of the A_g and E_g Raman mode of FeS₂ to 4.8 GPa and no Raman spectroscopic characterization of pyrite has been performed at pressures >5 GPa. We have recently shown that Raman scattering can be applied to high-pressure metallic phases in the 100 GPa range using the diamond-anvil cell (DAC) (Olijnyk and Jephcoat, 1999). Here we investigate the vibrational properties of natural iron pyrite with micro-Raman spectroscopy in the

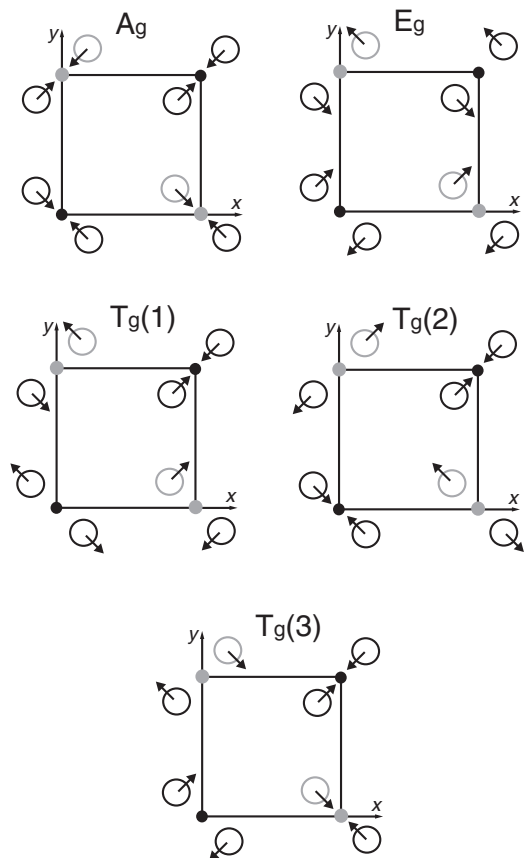


FIG. 1. Displacement vectors for the five Raman-active modes of FeS₂ pyrite (after Sourisseau *et al.*, 1991). Small, filled circles represent Fe atoms and the larger, hollow circles, the S atoms.

DAC to 55 GPa, comparing measurements made under hydrostatic conditions with helium as a pressure-transmitting medium and non-hydrostatic conditions (no pressure-transmitting medium) in order to determine any possible influence of the applied stress state on the vibrational properties of FeS₂. We also report the use of Zn as an internal pressure gauge in optical experiments.

Experiment

Two high-pressure micro-Raman spectroscopic experiments were performed on natural FeS₂ pyrite. In the ‘hydrostatic’ run an ~12 μm thick chip of a single-crystal of FeS₂, ~20 × 30 μm in size, was mounted in a diamond-anvil cell together with a 10 μm diameter ruby sphere for pressure calibration (Mao *et al.*, 1978). Culets of 400 μm diameter compressed a fully hardened T301 stainless steel gasket preindented to 40 μm with a 110 μm drilled hole. Fluid helium was loaded at 0.2 GPa (Jephcoat *et al.*, 1987) as a pressure-transmitting medium to ensure the best possible hydrostatic conditions. In a second, non-hydrostatic run a fine-grained powder sample was prepared by grinding pyrite crystals under ethanol. Culets of 300 μm in diameter and a stainless steel gasket preindented to 35 μm with a 100 μm hole formed the sample chamber. Compacted pyrite powder was loaded without a pressure-transmitting medium in order to maximize the stress gradient across the sample. In this non-hydrostatic run we placed a 2.5 μm thick and 20–25 μm wide Zn-foil strip on top of the pyrite powder across the centre of the hole (Fig. 2) to utilize the Raman-active E_{2g} mode of Zn as a pressure sensor (see below). Unpolarized Raman spectra to 51 GPa (hydrostatic run) and 55.2 GPa (non-hydrostatic run) were measured in 135° scattering geometry with a SPEX Triplemate equipped with a back-illuminated liquid-N₂-cooled CCD detector. Data were recorded for both increasing and decreasing pressure, and in the non-hydrostatic run at the centre and the edge of the sample chamber. The spectra were excited by the 514.5 nm line of an argon-ion laser focused to a 5 μm spot on the sample (with powers low enough to avoid heating the sample) and collected through a spatially-filtering (confocal) aperture giving high spatial resolution at the sample. The intrinsic resolution of the spectrometer is 1.5 cm⁻¹ and calibrations are accurate to ±1 cm⁻¹.

Zinc as an optical pressure sensor

Olijnyk *et al.* (2000) reported the pressure dependence of the Raman-active doubly degenerate E_{2g} phonon mode of Zn to 58 GPa at 300 K using a diamond-anvil cell and the ruby fluorescence method as pressure scale. The E_{2g} mode of Zn is a single, sharp and intense line at 71.1 cm⁻¹ at ambient conditions. With increasing pressure this mode shifts to higher wavenumbers without significant intensity loss. No phase transition is known or expected to occur in the 100 GPa range. The measured frequency-pressure data of the E_{2g} mode can be expressed as

$$P = \frac{\delta_0}{\delta'_0} \left(1 - \left(\frac{\nu(P)}{\nu_0} \right)^{-\delta'_0/\delta_0^2} \right)$$

where $\nu_0 = 71.1 \text{ cm}^{-1}$, $\delta_0 = (\partial \ln \nu / \partial P)_{P=0} = 0.05315 \text{ GPa}^{-1}$, and $\delta'_0 = -0.00728 \text{ GPa}^{-2}$ (Olijnyk *et al.*, 2000) and provides a useful alternative to the ruby pressure scale for optical studies. The measured E_{2g} frequencies are determined within ±0.2 cm⁻¹, corresponding to ±0.05 GPa at 1 GPa and ±0.2 GPa at 55 GPa. The properties of the E_{2g} mode of Zn make the metal an ideal secondary pressure sensor with

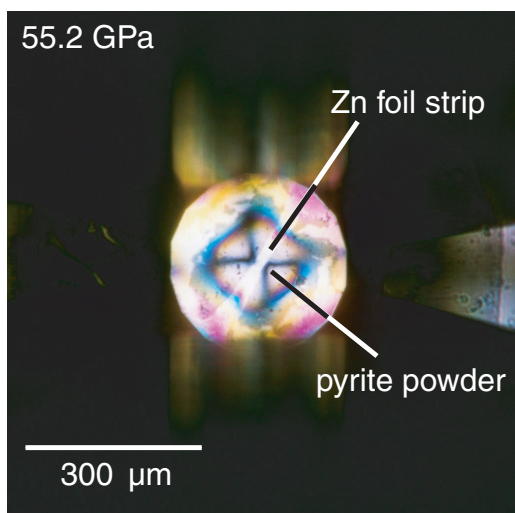


FIG. 2. View into the DAC through the cylinder diamond onto the non-hydrostatic pyrite powder sample with a Zn foil strip as pressure marker at 55.2 GPa in the centre of the sample chamber. The colourful pattern of birefringence develops when the diamond-anvils are stressed under pressure in polarized light.

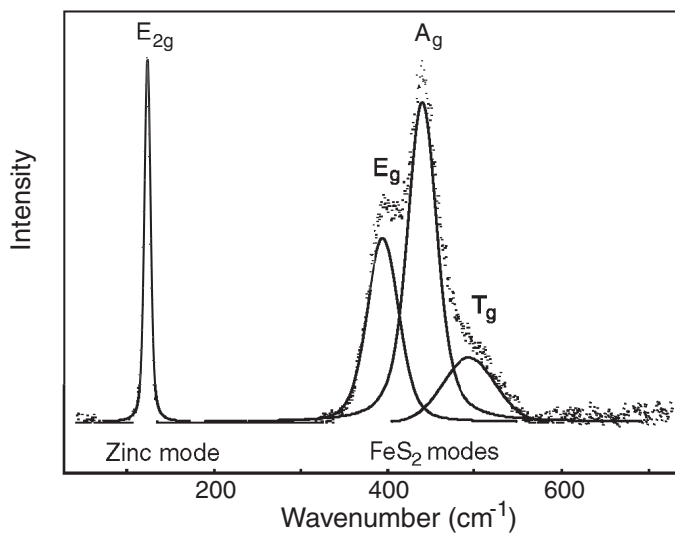


FIG. 3. Raman spectrum showing the modes of the Zn pressure marker and the pyrite sample under non-hydrostatic compression at 22.5 GPa.

distinct optical advantages especially in non-hydrostatic experiments. The metal does not contribute any broad-band emission to the Raman measurement and is optically clean. Furthermore, the frequency shift of the Zn phonon mode is insensitive to non-hydrostatic conditions and its half width remained $<12\text{ cm}^{-1}$ at pressures up to 55 GPa in the non-hydrostatic pyrite run. The E_{2g} mode of Zn was separated by $>250\text{ cm}^{-1}$ from the modes of the FeS_2 sample and did not interfere to the highest pressures. At various points across the sample, the Zn and FeS_2

modes were recorded together in one spectrum giving a precise local pressure (Fig. 3).

Results

Hydrostatic run

The ambient Raman spectrum of FeS_2 pyrite agrees well with previously published data (Table 1) (Mernagh and Trudu, 1993; Vogt *et al.*, 1983). Four modes are observed. The A_g and $T_g(2)$ mode occur $\leq 2\text{ cm}^{-1}$ apart (Vogt *et al.*, 1983) and cannot be resolved in the present

TABLE 1. Ambient Raman frequencies of the FeS_2 and their full width at half maximum (FWHM) under hydrostatic and non-hydrostatic compression. A comparison with literature data including mode assignment is given.

Present study				Vogt <i>et al.</i> (1983)	
ν_i (cm^{-1})	FWHM (cm^{-1}) at 1 bar	Hydrostatic FWHM (cm^{-1}) at 51 GPa	Non-hydrostatic FWHM (cm^{-1}) at 55.2 GPa	ν_i (cm^{-1})	Symmetries and assignment
344	3.2	9.2	30	343	E_g , S_2 libration
350	2.7	9.2		350	$T_g(1)$, coupled libration and stretch
				377	$T_g(2)$, S-S out-of-phase stretching
379	4.5	10	43	379	A_g , S-S in phase stretching
430	4.8	57*	60	430	$T_g(3)$, coupled libration and stretch

* at 39.6 GPa; at higher pressures the mode was a flat feature not easily fitted with a single peak (Fig. 4)

unpolarized, high-pressure Raman study. We observe a variation in the relative intensities of the Raman modes with changing orientation of the crystal relative to the incident laser beam, but this does not reveal the $T_g(2)$ mode. The spectra show only one peak at 379 cm^{-1} agreeing with the reported frequency of the A_g mode. The underlying $T_g(2)$ mode does not influence the fitted A_g peak position because its intensity is weak compared to the intensity of the A_g mode that dominates the spectrum. Under compression to 51 GPa, all modes shift continuously to higher frequencies (Figs 4, 5). Above 10 GPa, some

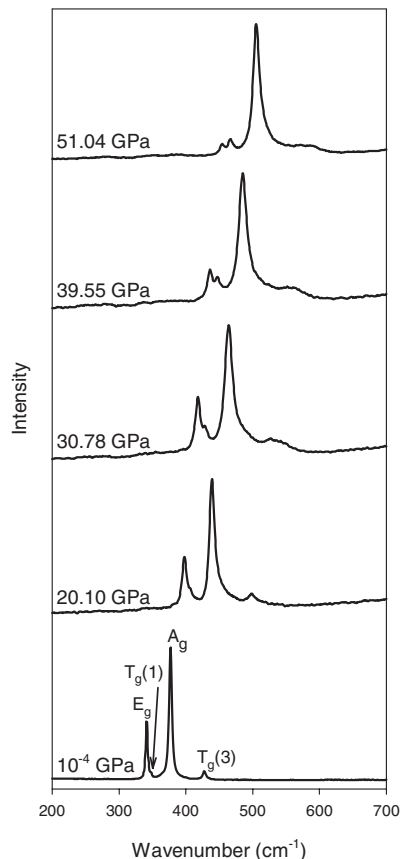


FIG. 4. Selected Raman spectra of FeS_2 pyrite with solid helium as the pressure-medium as a function of increasing pressure at 300 K. The ambient Raman spectrum was collected outside the DAC. Data are unsmoothed and no background was subtracted; rising background at higher wavenumbers is caused by the fluorescence of the diamond anvils and the internal scatter from the ruby.

spectra (e.g. at 14.9, 20.1 and 30.8 GPa) do show a weak and broad shoulder on the high-frequency side of the A_g mode. This shoulder seems to shift faster to higher frequencies than the A_g mode itself, but no pressure dependence can be established as it is not uniformly observed. The pressure dependence of the $T_g(1)$ mode is larger than that of the E_g mode ($2.91\text{ cm}^{-1}/\text{GPa}$ compared to $2.80\text{ cm}^{-1}/\text{GPa}$) leading to an increasing separation between them with pressure. The intensity of the E_g mode decreases relative to the intensity of the A_g and T_g modes with increasing pressure (using 514.5 nm laser excitation and fixed sample-to-laser beam orientation) particularly above 30 GPa. The full width at half maximum (FWHM) of the FeS_2 modes increases from $3\text{--}5\text{ cm}^{-1}$ to $\sim 10\text{ cm}^{-1}$ at 51 GPa (Fig. 6, Table 1). The $T_g(3)$ mode broadened more strongly and became a flat feature not easily fitted with a single peak at pressures above 40 GPa. We cannot exclude a splitting of the

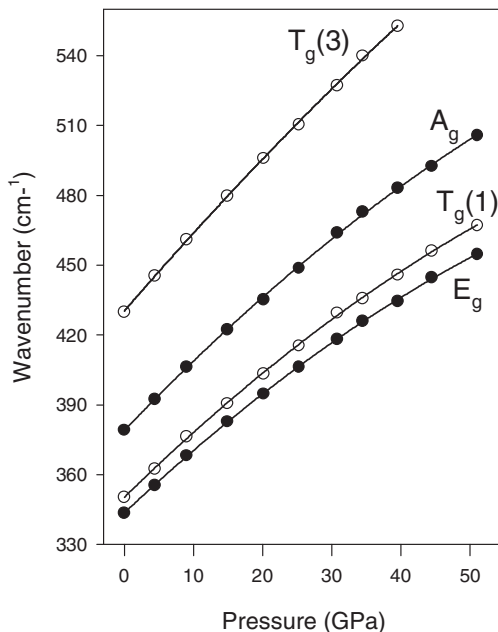


FIG. 5. Pressure dependence of the Raman modes of pyrite with helium as the pressure-transmitting medium. Errors in both frequency and pressure are within the size of the symbol. All modes were fitted with a weak quadratic term for the whole pressure range. For the $T_g(3)$ mode, only data up to 40 GPa are given because its weakness and large half width ($>50\text{ cm}^{-1}$) at higher pressures do not allow us to determine its frequency reliably.

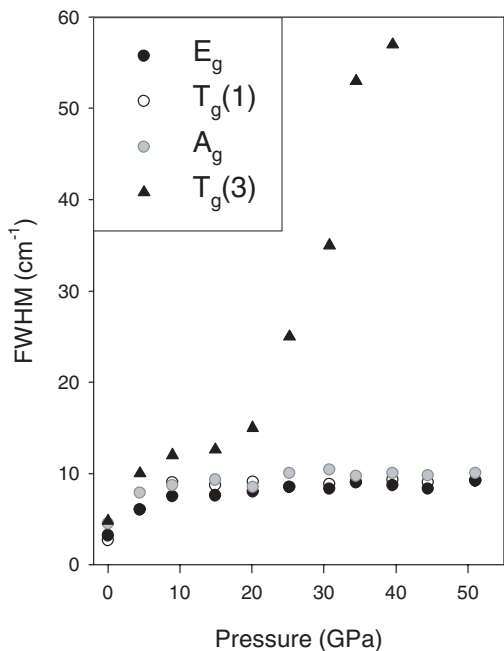


FIG. 6. Full width at half maximum (FWHM) of the Raman modes of pyrite with helium as the pressure-transmitting medium. Helium solidifies above 11 GPa at 300 K.

triply degenerate $T_g(3)$ mode due to the possible presence of small, non-hydrostatic stresses in the solid helium at pressures >12 GPa. Table 2 gives the pressure derivatives and mode Grüneisen parameters. The mode Grüneisen parameters $\gamma_{iT} = d \ln \nu_i / d \ln V$ were obtained from fitting the $\ln \nu_i(P)$ vs. $\ln V(P)$ values linearly. The $V(P)$ values were taken from Jephcoat (1985) using a Birch-

Murnaghan equation of state with bulk modulus $K_T = 133.5$ GPa and its pressure derivative $K'_T = 5.73$.

Non-hydrostatic run

The most obvious effect of non-hydrostaticity on the Raman spectrum of pyrite is the strong pressure-induced broadening of all modes (Fig. 7, Table 1). This substantial broadening of the modes leads to peak overlap and therefore lower resolution than in the hydrostatic run. The E_g and $T_g(1)$ modes are unresolvable at all pressures. We observe only one symmetric peak at a frequency that corresponds to the frequency of the more intense E_g mode in the hydrostatic run. With increasing pressure, the A_g and $T_g(3)$ mode gain in intensity relative to the E_g mode as is observed with helium as the pressure medium. Frequency-pressure data were collected from two different spots of the pyrite sample, close to the centre of the sample chamber and close to the edge of the gasket hole, in order to check for possible effects of different, local stress conditions on the FeS_2 modes and their pressure dependence. No detectable difference between the data collected at the centre and the edge of the gasket hole, either in the pressure dependence of the frequencies (Fig. 8) nor in the half widths of the modes was observed. Furthermore, the pressure dependence of the mode frequencies under non-hydrostatic and hydrostatic conditions agrees remarkably well within the errors of both measurements (Fig. 8, Table 2). The frequencies and half widths of the FeS_2 modes exhibit no hysteresis on pressure release and the ambient Raman spectra before and after the pressure application are identical.

TABLE 2. Pressure dependence and mode Grüneisen parameters of FeS_2 pyrite under hydrostatic and non-hydrostatic compression.

ν_i (cm^{-1})	Hydrostatic run to 51 GPa	γ_{i0}	Non-hydrostatic run to 55 GPa
	$\left(\frac{\partial \nu_i}{\partial P}\right)_T / \left(\frac{cm^{-1}}{GPa}\right)$		$\left(\frac{\partial \nu_i}{\partial P}\right)_T / \left(\frac{cm^{-1}}{GPa}\right)$
344	$2.80p - 1.21 \times 10^{-2}p^2$	1.36	$2.70p - 1.05 \times 10^{-2}p^2$
350	$2.91p - 1.20 \times 10^{-2}p^2$	1.39	
379	$3.10p - 1.20 \times 10^{-2}p^2$	1.40	$3.20p - 1.47 \times 10^{-2}p^2$
430	$3.43p - 8.36 \times 10^{-3}p^2$ *	1.42	$3.41p - 9.24 \times 10^{-3}p^2$

* to 39.6 GPa

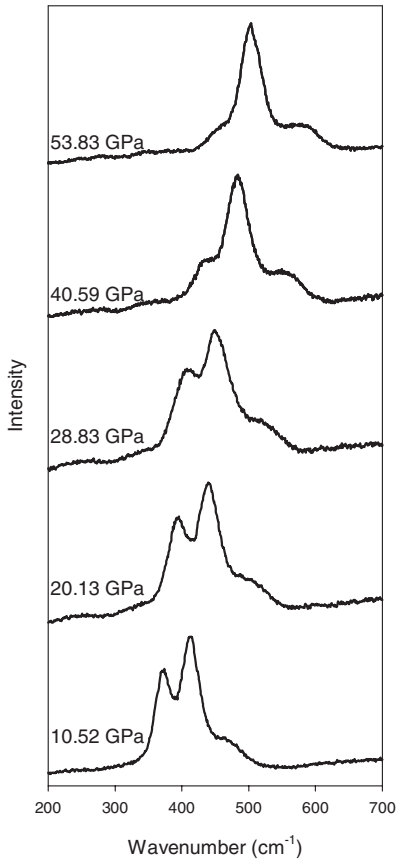


FIG. 7. Representative Raman spectra of non-hydrostatically compressed iron pyrite as a function of increasing pressure at 300 K. Data are unsmoothed and no background was subtracted.

Discussion and summary

The present study shows a continuous increase of all observed Raman frequencies of pyrite to the highest pressure of 55 GPa. There is no indication of a structural phase transition in FeS_2 in accord with high-pressure X-ray diffraction and shock-wave data (Merkel *et al.*, 2002; Ahrens and Jeanloz, 1987; Jephcoat, 1985). The mode Grüneisen parameters are very similar for all observed modes with the average mode Grüneisen parameter $\gamma_i = 1.39$ being close to the value of the thermal Grüneisen parameter of 1.59 (Ahrens and Jeanloz, 1987). The effect of pressure on the bond lengths in pyrite, S–S, Fe–S and Fe–Fe, is of fundamental interest regarding the properties of the band gap of FeS_2 . Eyert *et al.* (1998) showed,

based on first-principles calculations that small changes in the S–S bond length strongly influence position and width of the optical band gap. The observed positive pressure dependence of the stretching and librational mode frequencies of pyrite suggests a pressure-induced contraction of the S–S and Fe–S bonds, respectively. The frequency increase of the in-phase S–S stretching frequency (A_g) under compression is in accord with a shortening of the S–S bond length, because this stretching vibration is mainly determined by the S–S force constant (Lutz and Zwinscher, 1996). As the librational mode (E_g), and the coupled librational and stretching modes ($T_g(1,3)$), are largely governed by the Fe–S force constant (Lutz and Zwinscher, 1996; Sourisseau *et al.*, 1991), a pressure-induced increase in their mode frequencies agrees with a shortening of the Fe–S bond under compression. The effect of pressure on the S–S and Fe–S bond lengths in pyrite has been investigated previously with direct structural and theoretical methods: Fujii *et al.* (1986) reported single-crystal XRD data of FeS_2 to 4.2 GPa, and Sithole *et al.* (2003, 1999) calculated pressure-dependent bond lengths in pyrite. Both studies yielded a decrease in the S–S and Fe–S bond length under compression. On the other hand Will *et al.* (1984) reported a lengthening of the S–S bond from an energy-dispersive powder XRD experiment up to 40 GPa. The present, positive pressure dependence of the Raman modes of pyrite is compatible with a contraction of the S–S and Fe–S bond under compression. Non-hydrostatic conditions do not influence the pressure-induced frequency shifts of the Raman modes of iron pyrite within the experimental errors.

The striking gain in intensity of the A_g and $T_g(1)$ modes relative to the intensity of the E_g mode with increasing pressure is probably caused by inter-band resonance effects. Above band-gap (>0.9 eV) resonance Raman scattering from FeS_2 pyrite was first reported by Macfarlane *et al.* (1974). The authors observed a near order of magnitude increase in the intensity of the A_g mode on tuning the incident Ar^+ laser energies from 2.41 eV (514.5 nm) to 2.73 eV (454.6 nm). By coincidence, we also observe a near order of magnitude increase in the intensity ratios $I(A_g/E_g)$ and also $I(T_g(1)/E_g)$ by compressing FeS_2 to 51 GPa and probing with 514.5 nm excitation. Hence, to first order, pressure moves the resonance to lower energies, from ~ 2.73 eV at 1 bar to ~ 2.41 eV at 51 GPa. Macfarlane *et al.*

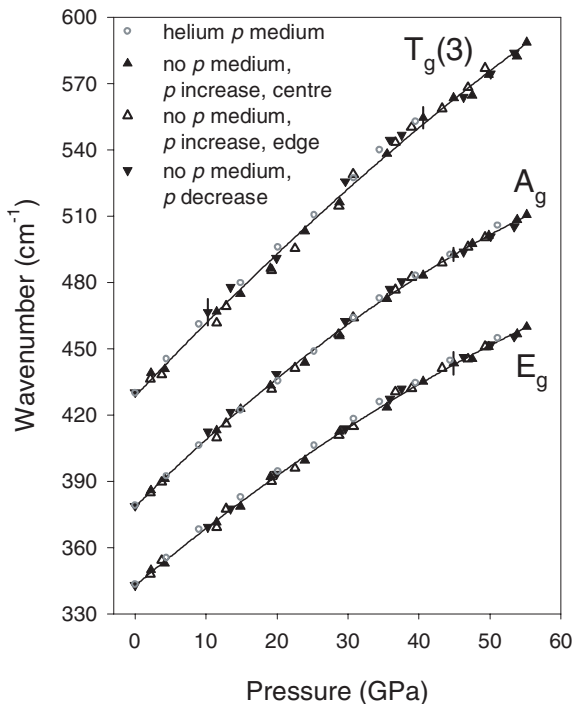


FIG. 8. Pressure dependence of the pyrite Raman modes. For comparison, data of the run with helium as a pressure-transmitting medium (grey circles) and without a pressure-medium (triangles) are shown. Filled triangles represent data measured close to the centre of the gasket hole and open triangles represent data measured close to the edge of the gasket hole. Representative error bars are given where the errors are larger than the symbol size. Solid lines are quadratic regressions to the non-hydrostatic data.

suggested that the resonance Raman scattering in FeS_2 is mainly caused by two direct inter-band electronic transitions occurring at 2.47 and 2.85 eV. Assuming that these inter-band transitions underlay the pressure-induced enhancement of the A_g and $T_g(1)$ intensity too, then the energy separation of the inter-bands involved in the resonance effect decreases with pressure, shifting the resonance towards lower excitation energies. Investigations of resonant Raman scattering of FeS_2 pyrite under pressure are underway and further study into the 100 GPa range, where metallization is expected, would also be worthwhile.

Acknowledgements

This work was supported by NERC fellowship NER/I/S/2001/00723 to AKK, NERC grant NER/B/S/200300258, and NERC grants GT59801ES and GR3/10912 to APJ. We thank an anonymous reviewer for comments.

References

- Ahrens, T.J. and Jeanloz, R. (1987) Pyrite: Shock compression, isentropic release, and composition of the Earth's core. *Journal of Geophysical Research*, **92**, 10,363–10,375.
- Anastassakis, E. and Perry, C.H. (1976) Light scattering and IR measurements in XS_2 pyrite-type compounds. *Journal of Chemical Physics*, **64**, 3604–3609.
- Cervantes, P., Slanic, Z., Bridges, F., Knittle, E. and Williams, Q. (2002) The band gap and electrical resistivity of FeS_2 -pyrite at high pressures. *Journal of Physics and Chemistry of Solids*, **63**, 1927–1933.
- Eyert, V., Höck, K.-H., Fiechter, S. and Tributsch, H. (1998) Electronic structure of FeS_2 : The crucial role of electron-lattice interaction. *Physical Review B*, **57**, 6350–6359.
- Ferrer, I.J., Nevskaja, D.M., de las Heras, C. and Sanchez, C. (1990) About the band gap nature of FeS_2 as determined from optical and photoelectrochemical measurements. *Solid State Communications*, **74**, 913–916.
- Fujii, T., Yoshida, A., Tanaka, K., Marumo, F. and

- Noda, Y. (1986) High pressure compressibilities of pyrite and catterite. *Mineralogical Journal*, **13**, 202–211.
- Jephcoat, A.P. (1985) *Hydrostatic compression studies on iron and pyrite to high pressures: the composition of the Earth's core and the equation of state of solid argon*. Ph.D. Thesis, John Hopkins Univ., Baltimore, Maryland.
- Jephcoat, A.P., Mao, H.-K. and Bell, P.M. (1987) Operation of the Megabar Diamond-Anvil Cell. Pp. 469–506 in: *Hydrothermal Experimental Techniques*, Wiley-Interscience, New York.
- Lutz, H.D. and Willich, P. (1974) Pyritestruktur -FIR-Spektren und Normalkoordinatenanalyse von MnS_2 , FeS_2 und NiS_2 . *Zeitschrift für anorganische und allgemeine Chemie*, **405**, 176–182.
- Lutz, H.D. and Zwinscher, J. (1996) Lattice dynamics of pyrite FeS_2 -polarizable-ion model. *Physics and Chemistry of Minerals*, **23**, 497–502.
- Macfarlane, R.M., Ushioda, S. and Blazey, K.W. (1974) Resonant Raman scattering from FeS_2 (pyrite). *Solid State Communications*, **14**, 851–855.
- Mao, H.-K., Bell, P.M., Shaner, J.W. and Steinberg, D.J. (1978) Specific volume measurements of Cu, Mo, Pd, and Ag and calibration of the ruby R_1 fluorescence pressure gauge from 0.06 to 1 Mbar. *Journal of Applied Physics*, **49**, 3276–3283.
- Merkel, S., Jephcoat, A.P., Shu, J., Mao, H.-K., Gillet, P. and Hemley, R.J. (2002) Equation of state, elasticity, and shear strength of pyrite under high pressure. *Physics and Chemistry of Minerals*, **29**, 1–9.
- Mernagh, T.P. and Trudu, A.G. (1993) A laser Raman microprobe study of some geologically important sulphide minerals. *Chemical Geology*, **103**, 113–127.
- Olijnyk, H. and Jephcoat, A.P. (1999) Effect of pressure on Raman spectra of metastable phases of Si and Ge. *Physica Status Solidi*, **B(211)**, 413–420.
- Olijnyk, H., Jephcoat, A.P., Novikov, D.L. and Christensen, N. (2000) Pressure shift of the zone-center TO mode of Zn. *Physical Review B*, **62**, 5508–5512.
- Opahle, I., Koepernik, K. and Eschrig, H. (1999) Full-potential band-structure calculation of iron pyrite. *Physical Review B*, **60**, 14,035–14,041.
- Sithole, H.M., Nguyen-Manh, D., Pettifor, D.G. and Ngoepe, P.E. (1999) Internal Relaxation, band gaps and elastic constant calculations of FeS_2 . *Molecular Simulation*, **22**, 31–37.
- Sithole, H.M., Ngoepe, P.E. and Wright, K. (2003) Atomistic simulation of the structure and elastic properties of pyrite (FeS_2) as a function of pressure. *Physics and Chemistry of Minerals*, **30**, 615–619.
- Sourisseau, C., Cavagnat, R. and Fouassier, M. (1991) The vibrational properties and valence force fields of FeS_2 , RuS_2 pyrites and FeS_2 marcasite. *Journal of Physics and Chemistry of Solids*, **52**, 537–544.
- Stevens, E.D., DeLucia, M.L. and Coppens, P. (1980) Experimental observation of the effect of crystal field splitting on the electron density distribution of iron pyrite. *Inorganic Chemistry*, **19**, 813–820.
- Takahashi, H., Minomura, S. and Mori, N. (1985) In *Abstract of the 26th High Pressure Conference in Japan*, pp. 20–21 (in Japanese).
- Ushioda, S. (1972) Raman scattering from phonons in iron pyrite (FeS_2). *Solid State Communications*, **10**, 307–310.
- Vogt, H., Chattopadhyay, T. and Stolz, H.J. (1983) Complete first-order Raman spectra of the pyrite structure compounds FeS_2 , MnS_2 and SiP_2 . *Journal of Physics and Chemistry of Solids*, **44**, 869–873.
- Will, G., Lauterjung, J., Schmitz, H. and Hinze, E. (1984) The bulk moduli of 3d-transition element pyrites measured with synchrotron radiation in a new belt type apparatus. Pp. 49–53 in: *High Pressure in Science and Technology*, volume **22** of Materials Research Society Symposia Proceedings.

[Manuscript received 11 November 2003;
revised 14 February 2004]